

Article

# Thermal Characteristics of Plastic Film Tension in Roll-to-Roll Gravure Printed Electronics

Kui He <sup>1,3</sup> , Shanhui Liu <sup>2,\*</sup>, Kedian Wang <sup>1</sup> and Xuesong Mei <sup>1</sup>

<sup>1</sup> School of Mechanical Engineering, Xi'an Jiaotong University, Xi'an 710049, Shaanxi, China; nyhekui@126.com (K.H.); 18736368618@126.com (K.W.); xameixs@hotmail.com (X.M.)

<sup>2</sup> Faculty of Printing, Packaging Engineering and Digital Media Technology, Xi'an University of Technology, Xi'an 710048, Shaanxi, China

<sup>3</sup> School of Mechanical Engineering, Henan University of Science and Technology, Luoyang 471003, Henan, China

\* Correspondence: shanhuiliu@xaut.edu.cn; Tel.: +86-159-2972-4880

Received: 17 January 2018; Accepted: 14 February 2018; Published: 23 February 2018

**Abstract:** In the printing section of a roll-to-roll gravure printed electronics machine, the plastic film tension is directly associated with the product quality. The temperature distribution of the plastic film in the printing section is non-uniform, because of the higher drying temperature and the lower room temperature. Furthermore, the drying temperature and the room temperature are not constants in industrial production. As the plastic film is sensitive to temperature, the temperature of the plastic film will affect the web tension in the printing section. In this paper, the thermal characteristics of the plastic film tension in roll-to-roll gravure printed electronics are studied in order to help to improve the product quality. First, the tension model including the factor of temperature is derived based on the law of mass conservation. Then, some simulations and experiments are carried out in order to in-depth research the effects of the drying temperature and room temperature based on the relations between system inputs and outputs. The results show that the drying temperature and room temperature have significant influences on the web tension. The research on the thermal characteristics of plastic film tension would benefit the tension control accuracy for further study.

**Keywords:** printed electronics; tension model; web tension; thermal characteristics; room temperature; drying temperature

## 1. Introductions

Printed electronics refers to the application of printing technologies for the fabrication of electronic circuits and devices. Roll-to-roll gravure printed electronics have received increasing attention in recent years because of its distinctive advantages, including: large surface area, flexible, customizable, low cost, and environmentally friendly. Though printing resolution and accuracy are not as high as conventional semiconductor fabrication, the above advantages are enough to warrant many new applications, such as Radio Frequency Identification (RFID) tags, thin film transistors, solar cells, touch screens, flexible displays, and light emitting devices.

Similar to conventional gravure printing processes, some kinds of conductive inks are printed on the moving substrate in sequence in order to achieve the desired functionality in roll-to-roll gravure printed electronics. The gravure printing system can be divided into three main sections: unwinding, printing, and rewinding. The web tension system exists in all the three sections. There are different requirements for web tension in the three sections, because of the different technical requirements. Some researchers have focused their works on the unwinding and rewinding sections [1–7]. In these research works, the unwinding tension model and rewinding tension model were studied, and then various kinds of control algorithms were adopted in order to achieve higher tension precision.

The control algorithms for unwinding or rewinding tension include Back Propagation (BP) neural network control [1], active disturbance rejection control (ADRC) [2], Fixed-Order  $H_{\infty}$  control [3], fuzzy adaptive Proportional-Integral-Differential (PID) control [4], Non-linear sliding-mode control [5], adaptive gain control [6], and so on.

In the printing section, the tension system and the register system are coupled together. Some research works are about the register model and register control algorithm, but these research works are based on the conventional tension model of a roll-to-roll web printing system [8–11]. Some research groups have studied the web tension system in the printing section, and the tension control algorithm is the research priority. Choi's group used a back stepping-based control algorithm and fuzzy decoupling method to reduce the propagation of tension disturbances in the roll-to-roll system [12,13]. Knittel's group analyzed the influence of the master roller placement, velocity, and tension bandwidths on the web tension of roll-to-roll systems [14], and then they developed a three-dimensional (3D) finite element model of the web and applied a robust control algorithm to control the web tension [15].

The aforementioned research works do not take into account the thermal effects in a roll-to-roll printing section. In fact, the effects of temperature on the tension system and register system in a gravure printing section are remarkable, and have attracted some researchers' attention recently. Pagilla's group developed a model to determine the temperature distribution in moving webs due to heating by radiation panels [16,17]. Shin's group studied the tension behavior through considering the thermal effects in roll-to-roll E-printing [18], and then researched the dynamic thermal characteristic of the register of roll-to-roll multi-layer printing systems [19].

Even so, the research on the thermal characteristics of plastic film tension is not sufficient. There is a lack of the research on the effects of room temperature and drying temperature on web tension in gravure printed electronics. In the printing section of a gravure printing machine, there are some drying devices behind the printing rollers for drying the printed conductive ink on the substrate. Usually, the web temperature outside the drying devices always changes with the room temperature, and the web temperature inside the drying devices always changes with the drying temperature. The range of the room temperature is from 10 °C to 30 °C, and the drying temperature is usually from 120 °C to 150 °C for nanosilver conductive ink. As the Polyethylene terephthalate (PET) material is sensitive to the temperature, and the Young's modulus of PET will decrease with the rise of the web temperature. It is obviously that the changes of the room temperature and drying temperature would affect the web tension by the Young's modulus of the web material. Some new issues about the tension system arise with the higher drying temperature and longer drying time in gravure printed electronics. With the higher requirement for printing quality, the effects of the room temperature and drying temperature on web tension need to be studied more deeply in order to obtain the thermal characteristics of the web tension, which will help to improve the tension control precision.

In this paper, we first set up the mathematical model of the web tension between two adjacent printing rollers through considering the room temperature and drying temperature. Then, some numerical simulations and experiments are carried out in order to study the effects of room temperature and drying temperature on the plastic film tension based on the relations between subsystem inputs and outputs. At last, the thermal characteristics of plastic film tension are summarized according to the simulations and experiments.

## 2. Tension Model Considering Temperature

The schematic diagram of a gravure printed electronics machine is shown in Figure 1. The gravure printed electronics machine is mainly composed of three sections: unwinding, printing, and rewinding. In printing section, each printing roller is driven by an independent servo motor. Two dancer rollers are installed in unwinding and rewinding sections for reducing web tension fluctuations and measuring tension signals. Load cells are set up in the web spans for measuring the web tensions, too. Photoelectric sensors are installed in the printing section for detecting register errors. Drying devices are set up

behind each printing roller for drying the conductive ink. The web tension system and the register system are coupled together in the printing section.

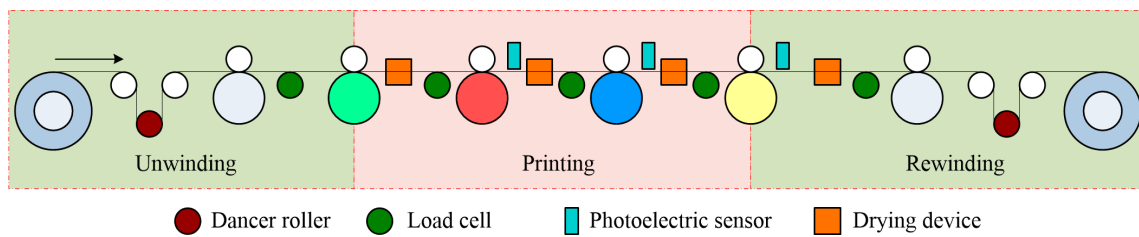


Figure 1. Diagram of a roll-to-roll gravure printed electronics machine.

Figure 2 shows the schematic diagram of the printing subsystem in the gravure printed electronics machine. The subsystem includes two printing units, a web, and a drying device, which is set between the two adjacent printing units for drying the printed conductive ink.  $T_{i-1}$  and  $T_i$  are the web tensions of the web spans.  $v_{i-1}$  and  $v_i$  are the tangential velocities of the printing rollers.  $L_i$  is the web length between two adjacent printing rollers.  $L_{Di}$  is the web length inside the drying device. In this web tension subsystem,  $T_{i-1}$ ,  $v_{i-1}$  and  $v_i$  are inputs,  $T_i$  is the output, and other parameters can be considered as influence factors. The subsystem is a typical Multiple-Input Single-Output (MISO) system.

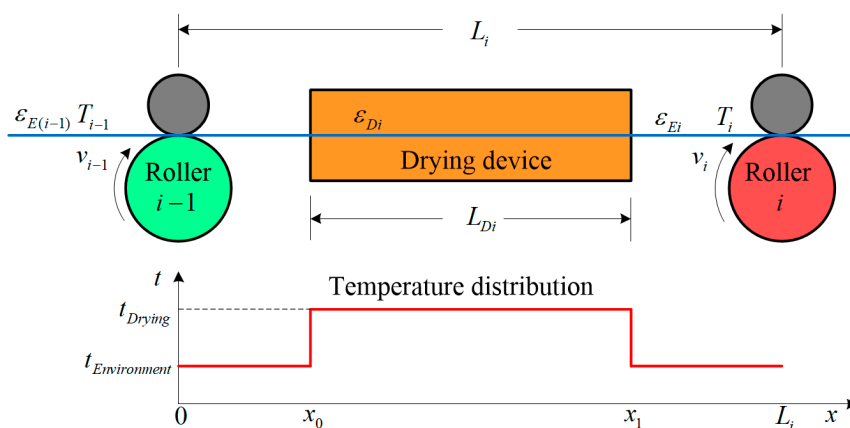


Figure 2. Schematic diagram of the printing subsystem.

Because of the existing of a drying device in the web span, the distribution of web temperature is not uniform. The web temperature inside the drying device is much higher than that outside the drying device. As the web is very thin and the heat-transfer process is fast, the duration of heat transfer can be considered as zero. Therefore, it can be considered that the web temperature inside the drying device is equal to the drying temperature, and the web temperature outside the drying device is equal to the room temperature. The web temperature distribution in a web span is shown in Figure 2.

For the web span between two adjacent printing rollers, the variation of the web mass is equal to the difference between the enter web mass and the exported web mass in unit time, i.e., the law of conservation of web mass. Based on the law of conservation of web mass, the mass conservation equation for the web span in Figure 2 can be obtained as follows:

$$\Delta m_i = m_{i[in]} - m_{i[out]}. \tag{1}$$

The detailed mass conservation equation can be get by substituting  $m = \rho V$  into Equation (1):

$$\frac{d}{dt} \left[ \int_0^{L_i} \rho_i(x, t) A_i(x, t) dx \right] = \rho_{i-1}(L_{i-1}, t) A_{i-1}(L_{i-1}, t) v_{i-1}(t) - \rho_i(L_i, t) A_i(L_i, t) v_i(t). \tag{2}$$

where  $\rho$  indicates the web density,  $A$  indicates the cross-sectional area of the web, and  $x$  indicates the position in the web span along the web motion direction.

Assuming the web material is perfectly elastic, the mass of a web element will not change with the stretched state, i.e.,

$$\rho A dx = \rho_u A_u dx_u. \tag{3}$$

where the subscript  $u$  indicates the un-stretched state of the web. Using the definition of strain, Equation (3) can be written as:

$$\frac{\rho A}{\rho_u A_u} = \frac{dx_u}{dx} = \frac{1}{1 + \varepsilon}. \tag{4}$$

where  $\varepsilon$  indicates the web strain in the web motion direction. Combining the Equations (2) and (4), we have

$$\frac{d}{dt} \left[ \int_0^{L_i} \frac{\rho_{ui}(x, t) A_{ui}(x, t)}{1 + \varepsilon_i(x, t)} dx \right] = \frac{\rho_{u(i-1)}(L_{i-1}, t) A_{u(i-1)}(L_{i-1}, t) v_{i-1}(t)}{1 + \varepsilon_{i-1}(L_{i-1}, t)} - \frac{\rho_{ui}(L_i, t) A_{ui}(L_i, t) v_i(t)}{1 + \varepsilon_i(L_i, t)}. \tag{5}$$

The web density and cross-sectional area in the un-stretched state do not change with the position and time, so we get:

$$\rho_{ui}(x, t) A_{ui}(x, t) = \rho_{u(i-1)}(L_{i-1}, t) A_{u(i-1)}(L_{i-1}, t) = \rho_{ui}(L_i, t) A_{ui}(L_i, t). \tag{6}$$

Based on Equation (6), Equation (5) can be written as:

$$\frac{d}{dt} \left[ \int_0^{L_i} \frac{1}{1 + \varepsilon_i(x, t)} dx \right] = \frac{v_{i-1}(t)}{1 + \varepsilon_{i-1}(L_{i-1}, t)} - \frac{v_i(t)}{1 + \varepsilon_i(L_i, t)}. \tag{7}$$

Because of the non-uniformity of the web temperature, the strain of the web is not uniform within the web span for a given web tension value. The web span can be divided into three parts according to the temperature distribution. So:

$$\int_0^{L_i} \frac{1}{1 + \varepsilon_i(x, t)} dx = \int_0^{x_0} \frac{1}{1 + \varepsilon_i(x, t)} dx + \int_{x_0}^{x_1} \frac{1}{1 + \varepsilon_i(x, t)} dx + \int_{x_1}^{L_i} \frac{1}{1 + \varepsilon_i(x, t)} dx. \tag{8}$$

The drying temperature is uniformity inside the drying device, so  $\varepsilon_i(x, t) = \varepsilon_{Di}(t)$ . Similarly, Outside the drying device,  $\varepsilon_i(x, t) = \varepsilon_{Ei}(t)$ . So, Equation (8) can be written as:

$$\int_0^{L_i} \frac{1}{1 + \varepsilon_i(x, t)} dx = \int_0^{x_0} \frac{1}{1 + \varepsilon_{Ei}(t)} dx + \int_{x_0}^{x_1} \frac{1}{1 + \varepsilon_{Di}(t)} dx + \int_{x_1}^{L_i} \frac{1}{1 + \varepsilon_{Ei}(t)} dx. \tag{9}$$

Calculating the integral parts:

$$\int_0^{L_i} \frac{1}{1 + \varepsilon_i(x, t)} dx = \frac{L_i(t) - L_{Di}(t)}{1 + \varepsilon_{Ei}(t)} + \frac{L_{Di}(t)}{1 + \varepsilon_{Di}(t)}. \tag{10}$$

Combining the Equations (7) and (10), we have:

$$\frac{d}{dt} \left[ \frac{L_i(t) - L_{Di}(t)}{1 + \varepsilon_{Ei}(t)} + \frac{L_{Di}(t)}{1 + \varepsilon_{Di}(t)} \right] = \frac{v_{i-1}(t)}{1 + \varepsilon_{E(i-1)}(t)} - \frac{v_i(t)}{1 + \varepsilon_{Ei}(t)}. \tag{11}$$

where  $\varepsilon_E$  indicates the web strain at room temperature outside the drying device, and  $\varepsilon_D$  indicates the web strain at the drying temperature inside the drying device.

As the strain  $\varepsilon$  is very small, so:

$$\frac{1}{1 + \varepsilon} \approx 1 - \varepsilon. \tag{12}$$

Substituting Equation (12) into Equation (11), Equation (13) can be obtained,

$$\frac{d}{dt} \{ [L_i(t) - L_{Di}(t)][1 - \varepsilon_{Ei}(t)] + L_{Di}(t)[1 - \varepsilon_{Di}(t)] \} = [1 - \varepsilon_{E(i-1)}(t)]v_{i-1}(t) - [1 - \varepsilon_{Ei}(t)]v_i(t). \quad (13)$$

Because the mechanical structure and the web path are fixed, so the changes of the web length  $L_i$  and  $L_{Di}$  can be ignored. Equation (13) can be written as:

$$-(L_i - L_{Di}) \frac{d}{dt} [\varepsilon_{Ei}(t)] - L_{Di} \frac{d}{dt} [\varepsilon_{Di}(t)] = [1 - \varepsilon_{E(i-1)}(t)]v_{i-1}(t) - [1 - \varepsilon_{Ei}(t)]v_i(t). \quad (14)$$

In practical applications, the drying temperature and room temperature are generally fixed. For the whole web span, the strain caused by thermal expansion and shrinkage is constant, although the moving web will generate thermal expansion and shrinkage at different positions of the web span. The thermal strain can be considered as a structure parameter, and it is compensated in the initial adjustment of the system. In this case, the constant thermal stain would not affect the web tension. So, the stain  $\varepsilon$  is generally caused by the tension. Using Hooker’s law,  $T = AE\varepsilon$ , we have:

$$-\frac{L_i - L_{Di}}{A_{Ei}E_{Ei}} \frac{dT_i(t)}{dt} - \frac{L_{Di}}{A_{Di}E_{Di}} \frac{dT_i(t)}{dt} = [1 - \frac{T_{i-1}(t)}{A_{E(i-1)}E_{E(i-1)}}]v_{i-1}(t) - [1 - \frac{T_i(t)}{A_{Ei}E_{Ei}}]v_i(t). \quad (15)$$

where  $E_E$  indicates the Young’s modulus of the web at room temperature, and  $E_D$  indicates the Young’s modulus of the web at drying temperature. The room temperatures outside the drying device are equal everywhere, so  $E_E = E_{E(i-1)} = E_{Ei}$ . Assuming that the drying temperatures of all of the drying devices are same ( $E_D = E_{D(i-1)} = E_{Di}$ ), and neglecting the changes of web cross-sectional area ( $A = A_{Di} = A_{E(i-1)} = A_{Ei}$ ), we have:

$$-\frac{L_i - L_{Di}}{AE_E} \frac{dT_i(t)}{dt} - \frac{L_{Di}}{AE_D} \frac{dT_i(t)}{dt} = [1 - \frac{T_{i-1}(t)}{AE_E}]v_{i-1}(t) - [1 - \frac{T_i(t)}{AE_E}]v_i(t). \quad (16)$$

Equation (16) can be written as:

$$[L_i + L_{Di}(\frac{E_E}{E_D} - 1)] \frac{dT_i(t)}{dt} = [AE_E - T_i(t)]v_i(t) - [AE_E - T_{i-1}(t)]v_{i-1}(t). \quad (17)$$

Equation (17) represents the mathematical model of the web tension between two adjacent printing rollers in a gravure printed electronics system.

### 3. Experimental Setup

The mathematical tension model of the roll-to-roll gravure printed electronics system shows that the temperature affects the web tension between two adjacent rollers by the web Young’s modulus at room temperature ( $E_E$ ), and the web Young’s modulus at drying temperature ( $E_D$ ). The web material (PET) is sensitive to temperature, so the web Young’s modulus  $E_E$  will change with the room temperature, and the web Young’s modulus  $E_D$  will change with the drying temperature.

For further studying the thermal characteristics of the plastic film tension in roll-to-roll printed electronics, the relations between the inputs and the outputs, including the room temperature and drying temperature, are researched through numerical simulations by using MATLAB/Simulink, and through experiments by using a gravure printing setup.

Figure 3 shows the gravure printed electronics experimental setup, which consists of three sections: unwinding, printing, and rewinding. In the printing section, all of the driving shafts are driven by servo motors (YASKAWA SGMGH-44), and the speeds of the printing rollers are obtained by the position encoders on the servo motor. Tension signals are picked up by load cells (MITSUBISHI LX-030TD) mounted on the idle rollers and then amplified by the tension amplifiers (MITSUBISHI LM-10TA).

The whole system is controlled by a multi-axis controller (GOOGOLTECH T8VME). The web material is PET.



Figure 3. Gravure printed electronics experimental setup.

In order to study the thermal characteristics, an open loop control system is adopted in order to control the printing roller speeds, and there is no tension controller in this section. There is a tension compensation setup near the load cell for compensating the decrease of the tension caused by the mechanical system (such as friction forces). The adjustment work occurs before production, and the compensation setup is not adjusted during production.

In Figure 2, setting  $i = 2$ , the model of the two adjacent printing rollers subsystems can be expressed as follows:

$$[L_2 + L_{D2}(\frac{E_E}{E_D} - 1)] \frac{dT_2(t)}{dt} = [AE_E - T_2(t)]v_2(t) - [AE_E - T_1(t)]v_1(t). \tag{18}$$

The mechanical parameters of the printing subsystem are summarized in Table 1.

Table 1. Mechanical Parameters of the Printing Subsystem.

Parameters	Values	Units
web length of a web span ( $L_2$ )	9.1	m
web length inside the drying device ( $L_{D2}$ )	3.5	m
web cross-sectional area ( $A$ )	$1 \times 10^{-4}$	m <sup>2</sup>

The room temperature range of the workshop is usually between  $\sim 10\sim 30$  °C, and the drying temperature range is usually from  $\sim 120\sim 150$  °C. As the web material is Polyethylene terephthalate (PET), the relations between web temperature and the Young’s modulus are shown in Table 2.

Table 2. Relations between Temperature and the Young’s modulus of Polyethylene terephthalate (PET).

Web Temperate (°C)	10	20	30	120	135	150
Young’s Modulus ( $10^9$ Pa)	5.200	4.890	4.590	0.622	0.463	0.365

The process parameters are as follows: the steady-state value of upstream web tension  $T_1^* = 100$  N, the steady speeds of the printing rollers  $v_1^* = v_2^* = 10$  m/min.

#### 4. Effects of Drying Temperature on Web Tension

##### 4.1. $T_1$ Is Input, $T_2$ Is Output, $v_1$ and $v_2$ Are Constants

$T_1(t)$  has step changes ( $\Delta T_1 = 10$  N) at 500 s when the drying temperatures are equal to 20 °C, 120 °C, 135 °C, and 150 °C, respectively, the step responses of the tension  $T_2(t)$  are shown in Figures 4 and 5. The step changes of  $T_1(t)$  cause the step changes of  $T_2(t)$ . The drying temperature affects the transient responses rather than the steady-state responses.

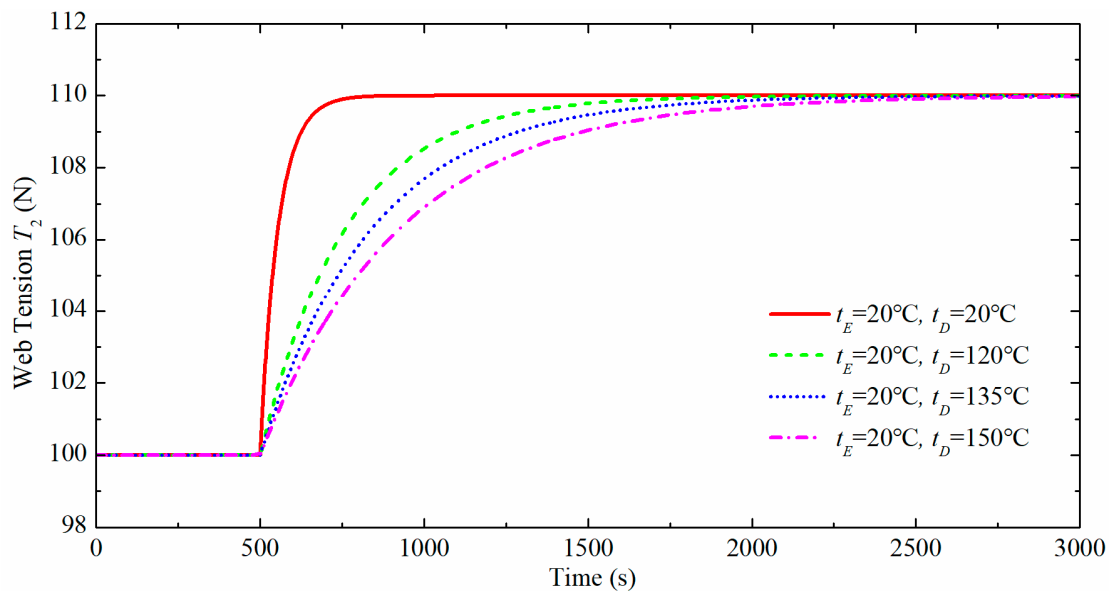


**Figure 4.** The responses of the tension  $T_2(t)$  as  $T_1(t)$  has step changes at different drying temperatures in simulations.

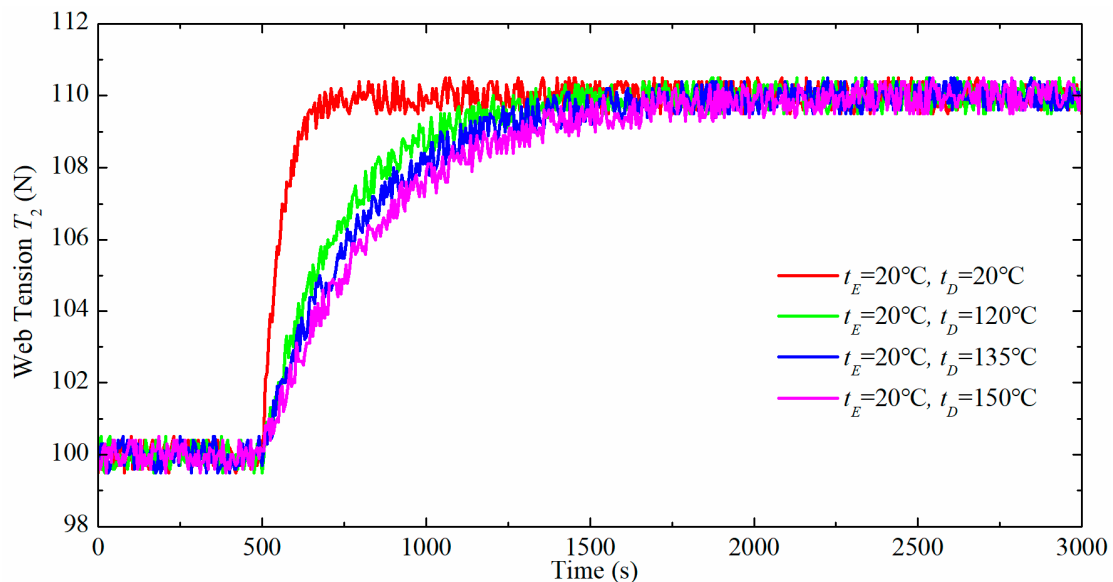


**Figure 5.** The responses of the tension  $T_2(t)$  as  $T_1(t)$  has step changes at different drying temperatures in experiments.

The steady-state values of  $T_2(t)$  increase 10 N as  $\Delta T_1 = 10$  N at different drying temperatures, i.e., the drying temperature does not affect the steady-state tension  $T_2(t)$  caused by input tension  $T_1(t)$ .

In the transient response, the settling time  $T_s$  is defined as the time required for the system to settle within a certain percentage  $\delta$  of the input amplitude, which is usually  $\delta = 2\%$ . In Figure 4, the settling times  $T_s$  are 202 s, 961 s, 1260 s, and 1574 s at 20 °C, 120 °C, 135 °C, and 150 °C, respectively. The ratios between the increases of the settling times  $\Delta T_s$  and the settling times  $T_s$  are about 31% and 25% when the dry temperatures vary from ~120~135 °C and ~135~150 °C, respectively. It shows that: first, the difference between the transient response without using the drying system, and the transient response using the drying system is very obvious, and the thermal effect of the drying system on tension can't be neglected; second, the settling times  $T_s$  increase with the increases of the values of the drying temperature, and the growth rate is about 30% for each 15 °C rise in the drying temperature.

#### 4.2. $v_1$ Is Input, $T_2$ Is Output, $T_1$ and $v_2$ Are Constants

$v_1(t)$  has step changes ( $\Delta v_1 = 0.001\text{m/min}$ ) at 500 s when the drying temperatures are equal to 20 °C, 120 °C, 135 °C, and 150 °C, respectively, the responses of the tension  $T_2(t)$  are shown in Figures 6 and 7. The step changes of  $v_1(t)$  cause the negative step changes of  $T_2(t)$ . The drying temperature only affects the transient response.

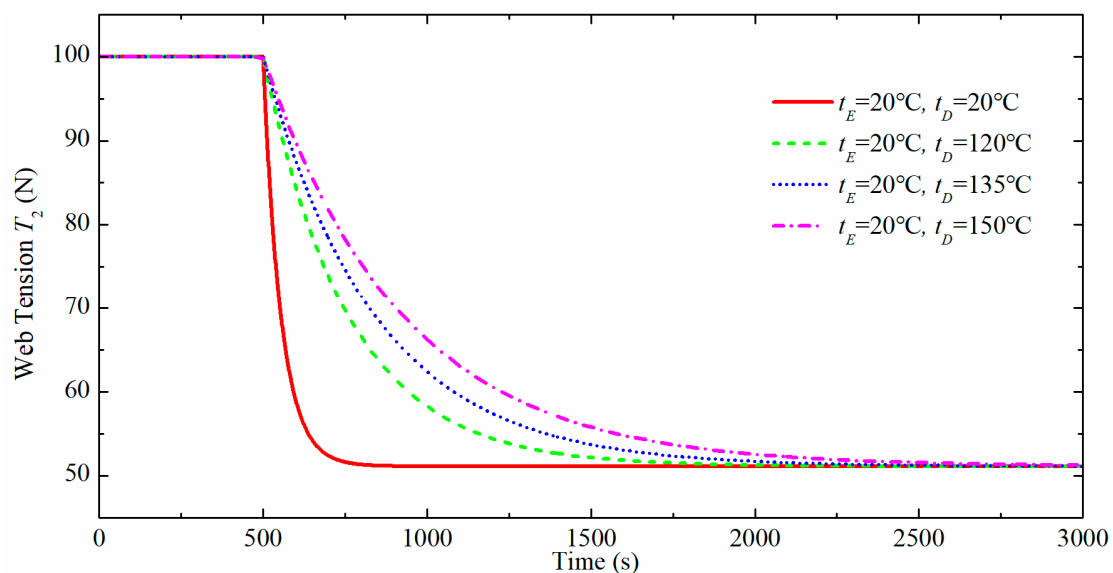


**Figure 6.** The responses of the tension  $T_2(t)$  as  $v_1(t)$  has step changes at different drying temperatures in simulations.

The steady-state values of  $T_2(t)$  decrease about 49 N as  $\Delta v_1 = 0.001\text{ m/min}$  at different drying temperatures, i.e., the drying temperature does not affect the steady-state tension  $T_2(t)$  caused by input velocity  $v_1(t)$ .

For the transient response in Figure 6, the settling times  $T_s$  are 202 s, 961 s, 1260 s, and 1574 s at 20 °C, 120 °C, 135 °C, and 150 °C, respectively. The values of the settling times  $T_s$  are the same to that in Section 4.1. It shows that: first, the difference between the transient response without the drying system and using the drying system is also obvious too; second, the settling times  $T_s$  increase with the increases of the values of the drying temperature.

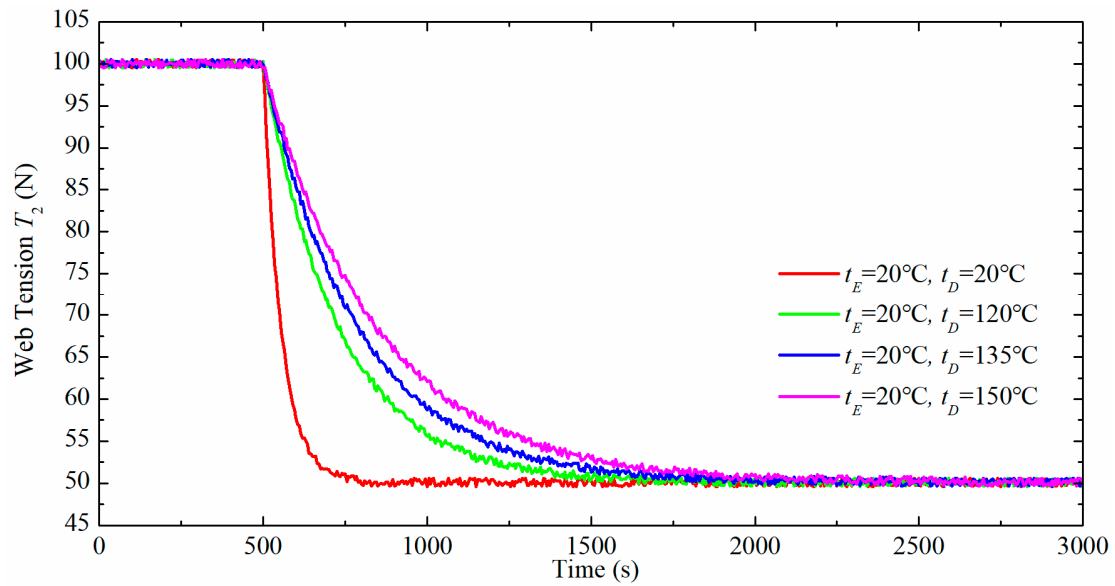


**Figure 7.** The responses of the tension  $T_2(t)$  as  $v_1(t)$  has step changes at different drying temperatures in experiments.

4.3.  $v_2$  Is Input,  $T_2$  Is Output,  $T_1$  and  $v_1$  Are Constants

$v_2(t)$  has step changes ( $\Delta v_2 = 0.001$  m/min) at 500 s when the drying temperatures are equal to 20 °C, 120 °C, 135 °C, and 150 °C, respectively, the responses of the tension  $T_2(t)$  are shown in Figures 8 and 9. The step changes of  $v_2(t)$  cause the step changes of  $T_2(t)$ . The value of the drying temperature only affects the transient response, which is similar to Section 4.2.

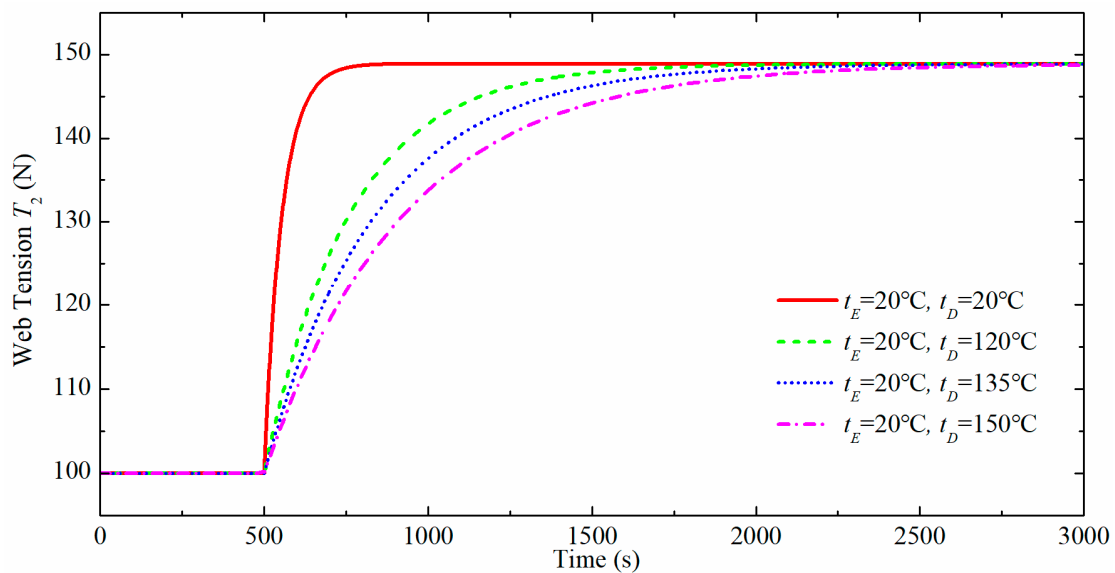


**Figure 8.** The responses of the tension  $T_2(t)$  as  $v_2(t)$  has step changes at different drying temperatures in simulations.

The steady-state values of  $T_2(t)$  increase about 49 N as  $\Delta v_2 = 0.001$  m/min at different drying temperatures, i.e., the drying temperature does not affect the steady-state tension  $T_2(t)$  caused by input velocity  $v_2(t)$ .

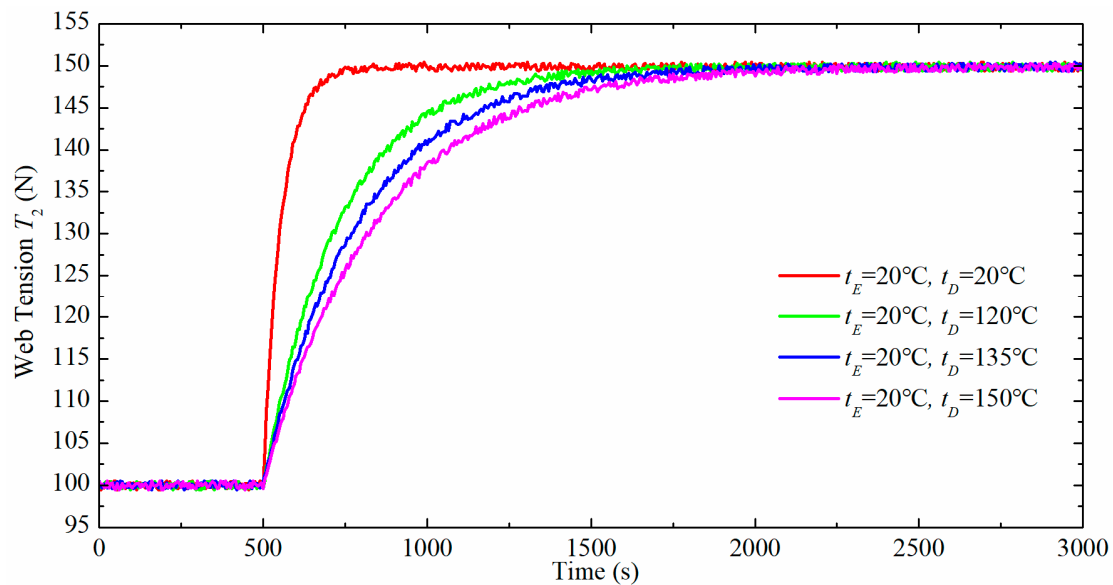


**Figure 9.** The responses of the tension  $T_2(t)$  as  $v_2(t)$  has step changes at different drying temperatures in experiments.

For the transient response in Figure 8, the settling times  $T_s$  are 202 s, 961 s, 1260 s, and 1574 s at 20 °C, 120 °C, 135 °C, and 150 °C, respectively. The values of the settling times  $T_s$  are the same to that in Sections 4.1 and 4.2. It shows that: first, the difference between the transient response without the drying system and the transient response when using the drying system is also obvious too; second, the settling times  $T_s$  increase with the increases of the values of the drying temperature.

## 5. Effects of Room Temperature on Web Tension

### 5.1. $T_1$ Is Input, $T_2$ Is Output, $v_1$ and $v_2$ Are Constants

$T_1(t)$  has step changes ( $\Delta T_1 = 10$  N) at 500 s when the room temperatures are equal to 10 °C, 20 °C, and 30 °C, respectively, the step responses of the tension  $T_2(t)$  are shown in Figures 10 and 11. The step changes of  $T_1(t)$  cause the step changes of  $T_2(t)$ . The room temperature affects the transient responses rather than the steady-state responses.

The steady-state values of  $T_2(t)$  increase 10 N as  $\Delta T_1 = 10$  N, respectively, at different room temperatures, i.e., the room temperature does not affect the steady-state tension  $T_2(t)$  caused by input tension  $T_1(t)$ .

For the transient response in Figure 10, the settling times  $T_s$  are 1334 s, 1260 s, and 1188 s at 10 °C, 20 °C, and 30 °C, respectively. The ratios between the decreases of the settling times  $\Delta T_s$  and the settling times  $T_s$  are  $-5.5\%$  and  $-5.7\%$  when the room temperatures vary from  $\sim 10\sim 20$  °C and  $\sim 20\sim 30$  °C, respectively. It shows that: first, the settling times  $T_s$  decrease with the increases of the values of room temperature; second, the settling times  $T_s$  decrease about 6% for each 10 °C rise in room temperature, which is a less obvious decline than that caused by the drying temperature.

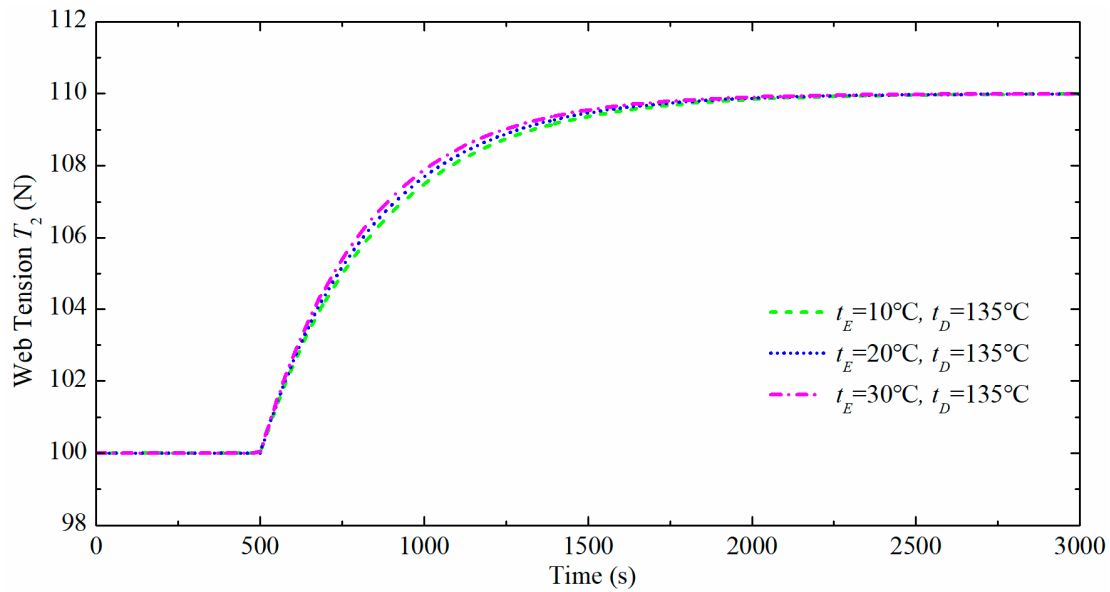


**Figure 10.** The responses of the tension  $T_2(t)$  as  $T_1(t)$  has step changes at different room temperatures in simulations.

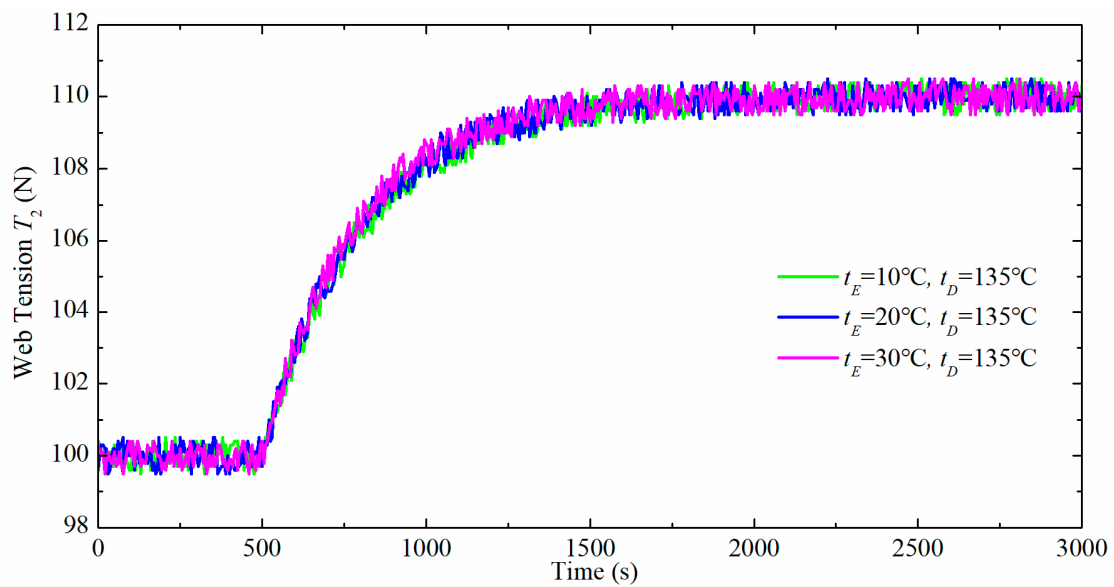


**Figure 11.** The responses of the tension  $T_2(t)$  as  $T_1(t)$  has step changes at different room temperatures in experiments.

5.2.  $v_1$  Is Input,  $T_2$  Is Output,  $T_1$  and  $v_2$  Are Constants

$v_1(t)$  has step changes ( $\Delta v_1 = 0.001$  m/min) at 500 s when the room temperatures are equal to 10 °C, 20 °C, and 30 °C, respectively, the responses of the tension  $T_2(t)$  are shown in Figures 12 and 13. The step changes of  $v_1(t)$  cause the negative step changes of  $T_2(t)$ . The room temperature affects both the steady-state response and the transient response.

For the steady-state response in Figure 12, the steady-state values of  $T_2(t)$  decrease 52.0 N, 48.9 N, and 45.9 N when the room temperatures are 10 °C, 20 °C, and 30 °C, respectively. It shows that the decreases of the steady-state values  $T_2(t)$  decrease with the rise of the room temperature, in other words, the steady-state values of  $T_2(t)$  caused by a certain step change of the input velocity  $v_1(t)$  in the step responses, increase with the increases of the room temperature. The differences between

the steady-state values of  $T_2(t)$  are 3.1 N and 3 N when the room temperatures vary from  $\sim 10\sim 20^\circ\text{C}$  and  $\sim 20\sim 30^\circ\text{C}$ , respectively. Furthermore, the ratios between the differences of the steady-state values of  $T_2(t)$  and the decreases of the steady-state values  $T_2(t)$  are 5.96% and 6.14% when the room temperatures vary from  $\sim 10\sim 20^\circ\text{C}$  and  $\sim 20\sim 30^\circ\text{C}$ , respectively. It shows that the steady-state values  $T_2(t)$  caused by a certain step change of the input velocity  $v_1(t)$  increase about 6% for each  $10^\circ\text{C}$  rise in room temperature, which would also make a measurable impact on precise tension control.

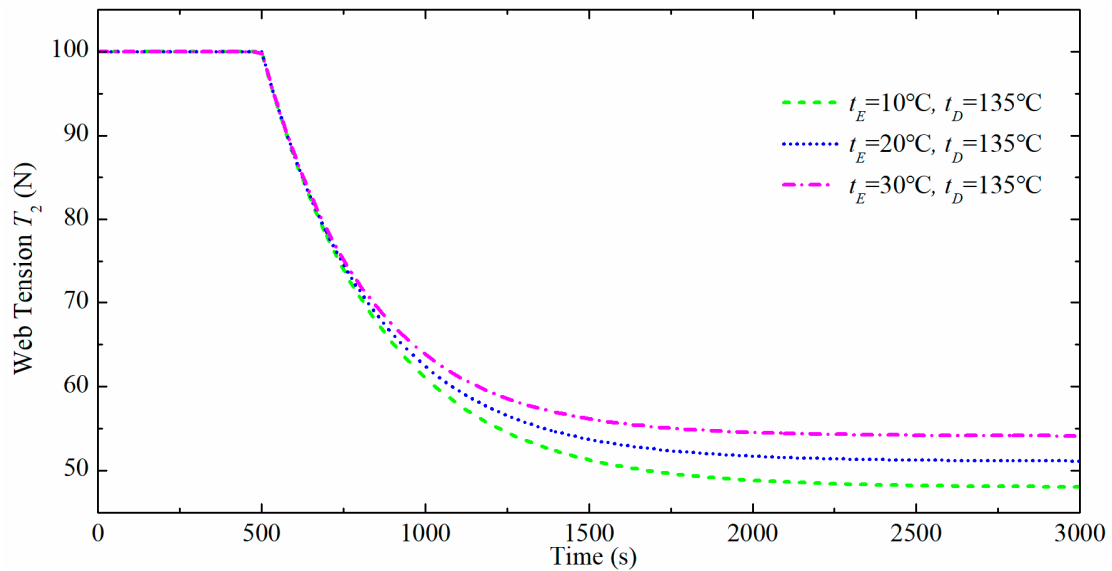


**Figure 12.** The responses of the tension  $T_2(t)$  as  $v_1(t)$  has step changes at different room temperatures in simulations.

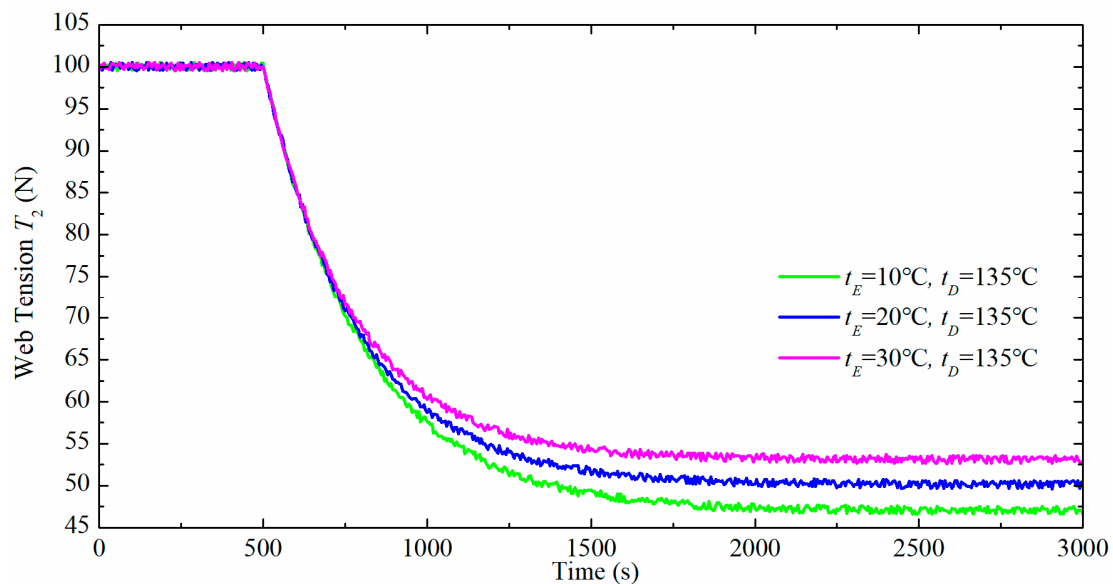


**Figure 13.** The responses of the tension  $T_2(t)$  as  $v_1(t)$  has step changes at different room temperatures in experiments.

For the transient response in Figure 12, the settling times  $T_s$  are 1334 s, 1260 s, and 1188 s at  $10^\circ\text{C}$ ,  $20^\circ\text{C}$ , and  $30^\circ\text{C}$ , respectively. Furthermore, the ratios between the decreases of the settling times  $\Delta T_s$  and the settling times  $T_s$  are  $-5.5\%$  and  $-5.7\%$  when the room temperatures vary from  $\sim 10\sim 20^\circ\text{C}$  and  $\sim 20\sim 30^\circ\text{C}$ , respectively. The results of the transient responses are the same to the step responses in

Section 5.1. The similar conclusions are as follows: the settling times  $T_s$  decrease with the increases of the room temperature, and the decrease rate is about 6% for each 10 °C rise in the room temperature.

5.3.  $v_2$  Is Input,  $T_2$  Is Output,  $T_1$  and  $v_1$  Are Constants

$v_2(t)$  has step changes ( $\Delta v_2 = 0.001$  m/min) at 500 s when the room temperatures are equal to 10 °C, 20 °C, and 30 °C, respectively, the responses of the tension  $T_2(t)$  are shown in Figures 14 and 15. The step changes of  $v_2(t)$  cause the step changes of  $T_2(t)$ . The value of the room temperature affects both the steady-state response and the transient response, which is similar to Section 5.2, but has the opposite results.

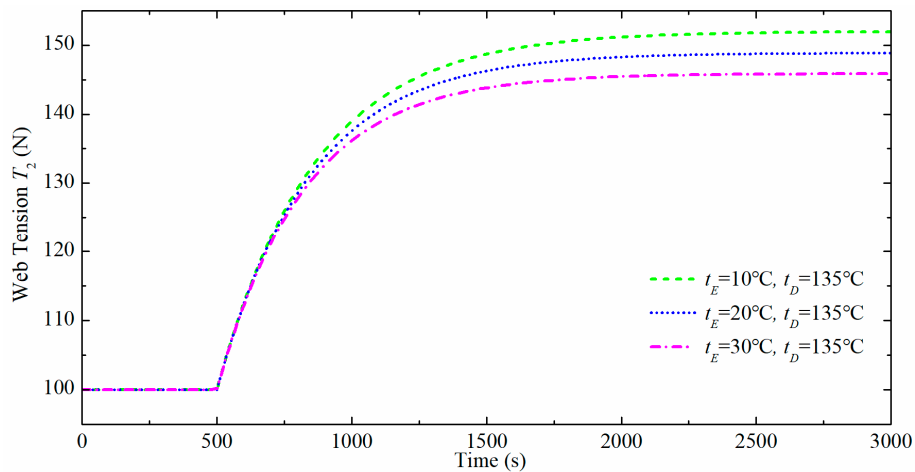


Figure 14. The responses of the tension  $T_2(t)$  as  $v_2(t)$  has step changes at different room temperatures in simulations.

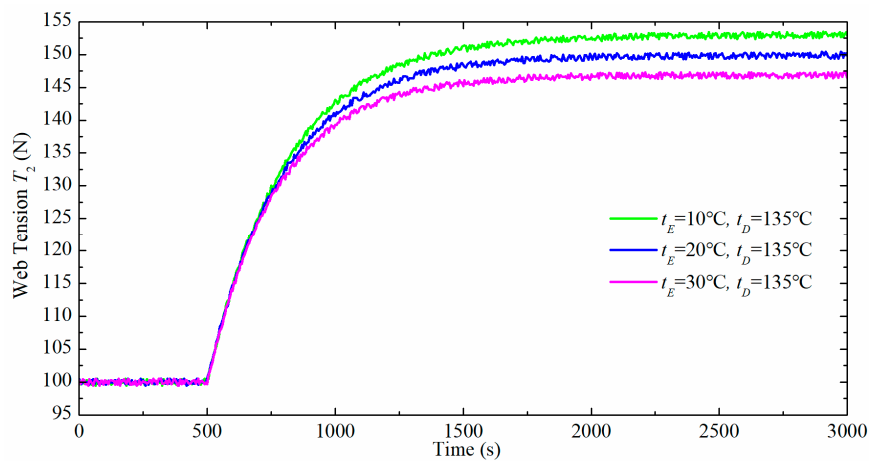


Figure 15. The responses of the tension  $T_2(t)$  as  $v_2(t)$  has step changes at different room temperatures in experiments.

For the steady-state response in Figure 14, the steady-state values of  $T_2(t)$  increase 52.0 N, 48.9 N, and 45.9 N when the room temperatures are 10 °C, 20 °C, and 30 °C, respectively. The values of the steady-state response are the same to the step responses in Section 5.2, so the conclusion is similar, too. The steady-state values of  $T_2(t)$  caused by a certain step change of the input velocity  $v_2(t)$  in the step responses, decrease with the increases of the values of room temperature, and the decrease rate is about 6% for each 10 °C rise in room temperature.

For the transient response in Figure 14, the settling times  $T_s$  are 1334 s, 1260 s, and 1188 s at 10 °C, 20 °C, and 30 °C, respectively. The ratios between the decreases of the settling times  $\Delta T_s$  and the settling times  $T_s$  are  $-5.5\%$  and  $-5.7\%$  when the room temperatures vary from  $\sim 10\sim 20$  °C and  $\sim 20\sim 30$  °C, respectively. Similarly, the settling times  $T_s$  decrease with the increases of the values of room temperature, and the decrease rate is about 6% for each 10 °C rise in room temperature.

## 6. Discussions

Through the aforementioned simulations and experiments, the thermal characteristics of the plastic film tension in roll-to-roll printed electronics are summarized as follows.

(1) The experimental results are according to that in the numerical simulations, and it shows the correctness of the mathematical model, including room temperature and drying temperature.

(2) The drying temperature does not affect the steady-state value of web tension, whatever the input type. The drying temperature obviously affects the transient process, and the settling time increases with the rise of drying temperature.

(3) The room temperature affects both the steady-state response and the transient response. For the steady-state response, the room temperature does not affect the steady-state value of web tension when the input is upstream web tension. When the input is roller velocity, the absolute change of the steady-state web tension decreases with the rise of the room temperature. For the transient response, the settling time decreases with the rise of the room temperature, which is the opposite of the drying temperature, furthermore, the change rate is much less than that caused by the drying temperature.

(4) For a given room temperature or drying temperature, the settling times are the same across the different input types and values.

(5) The settling time, considering the drying temperature, is about 5–8 times longer than that without considering the drying temperature, which means that the transient process can't be neglected, otherwise, the quality of the printed electronics during this time is not guaranteed.

(6) In practical applications, the drying temperature could be adjusted to compensate for the change of the transient process caused by the variation of room temperature. In this case, the speed of the hot air should be changed with the drying temperature in order to guarantee the drying quality.

(7) In order to reduce the effect of room temperature on web tension, a constant temperature workshop could be built to keep the room temperature constant.

## 7. Conclusions

To obtain higher printing precision, the thermal characteristics of plastic film tension in roll-to-roll gravure printed electronics need to be researched in-depth. In this paper, the tension model including a drying system is derived based on the law of mass conservation. The mathematical model shows that the drying temperature and the room temperature could affect the web tension by the thermal behavior of the plastic film. Then, the thermal effects of the drying temperature and the room temperature on web tension are studied by using numerical simulations and experiments based on the relations between system inputs and outputs. In the transient responses, the settling time increases with the rise of the drying temperature, but decreases with the rise of the room temperature, and the effect of the drying temperature is more obvious than that of the room temperature. In steady-state responses, only the room temperature affects the steady-state value of the web tension when the input is the velocity of the printing roller. Based on these thermal characteristics of the plastic film tension in roll-to-roll gravure printed electronics, it is conducive to adopt an appropriate control strategy in order to obtain a higher precision of register control in practical applications.

**Acknowledgments:** This project is supported by the National Natural Science Foundation of China (Grant No. 51505376), the Natural Science Basic Research Plan in Shaanxi Province of China (Grant No. 2016JQ5038), and Project funded by China Postdoctoral Science Foundation (Grant No. 2016M602844).

**Author Contributions:** Kedian Wang and Xuesong Mei conceived and designed the experiments; Kui He performed the experiments; Kui He and Shanhui Liu analyzed the data and wrote the paper.

**Conflicts of Interest:** The authors declare no conflict of interest.

## References

1. Li, J.; Mei, X.; Tao, T.; Liu, S. Design tension controller of unwinding system based on BP neural network. *Adv. Sci. Lett.* **2011**, *4*, 2222–2226. [[CrossRef](#)]
2. Liu, S.; Mei, X.; Kong, F.; He, K. A Decoupling Control Algorithm for Unwinding Tension System Based on Active Disturbance Rejection Control. *Math. Prob. Eng.* **2013**, *2013*, 1798–1803. [[CrossRef](#)]
3. Gassmann, V.; Knittel, D.; Pagilla, P.R.; Bueno, M. Fixed-Order  $H_\infty$  Tension Control in the Unwinding Section of a Web Handling System Using a Pendulum Dancer. *IEEE Trans. Control Syst. Technol.* **2011**, *20*, 173–180. [[CrossRef](#)]
4. Yang, M.; Zhang, S. The research of tension control system in web press based on the fuzzy adaptive PID controller. In Proceedings of the 2014 9th IEEE Conference on Industrial Electronics and Applications, Hangzhou, China, 9–11 June 2014; pp. 1204–1208.
5. Abjadi, N.R.; Soltani, J.; Askari, J.; Arab Markadeh, G.R. Nonlinear sliding-mode control of a multi-motor web-winding system without tension sensor. *IET Control Theory Appl.* **2009**, *3*, 419–427. [[CrossRef](#)]
6. Park, J.; Jeon, S.; Nam, K.; Liu, L.; Sun, J.; Kim, C. Tension control of web of winder span using adaptive gain control method. *Jpn. J. Appl. Phys.* **2014**, *53*, 05HC11. [[CrossRef](#)]
7. Shao, M.; Wu, J.; Wang, Y.; Fang, K.; Guo, X. Research on modeling method of winding tension system for gravure printing machine. In Proceedings of the 2016 Symposium on Piezoelectricity, Acoustic Waves, and Device Applications (SPAWDA), Xi'an, China, 21–24 October 2016; pp. 110–114.
8. Chen, Z.; He, J.; Zheng, Y.; Song, T.; Deng, Z. An Optimized Feedforward Decoupling PD Register Control Method of Roll-to-Roll Web Printing Systems. *IEEE Trans. Autom. Sci. Eng.* **2016**, *13*, 274–283. [[CrossRef](#)]
9. Chen, Z.; Zheng, Y.; Zhou, M.; Wong, D.; Chen, L.; Deng, Z. Model-based feedforward register control of roll-to-roll web printing systems. *Control Eng. Pract.* **2016**, *51*, 58–68. [[CrossRef](#)]
10. Li, J.; Mei, X.; Tao, T.; Liu, S. Research on the register system modelling and control of gravure printing press. *Proc. Inst. Mech. Eng. Part C J. Mech. Eng. Sci.* **2012**, *226*, 626–635. [[CrossRef](#)]
11. Liu, S.; Mei, X.; Li, J.; Ma, L. Machine Directional Register System Modeling for Shaft-Less Drive Gravure Printing Machines. *Math. Prob. Eng.* **2013**, *2013*, 206–226. [[CrossRef](#)]
12. Tran, T.; Choi, K. A backstepping-based control algorithm for multi-span roll-to-roll web system. *Int. J. Adv. Manuf. Technol.* **2014**, *70*, 45–61. [[CrossRef](#)]
13. Ponniah, G.; Zubair, M.; Doh, Y.; Choi, K. Fuzzy decoupling to reduce propagation of tension disturbances in roll-to-roll system. *Int. J. Adv. Manuf. Technol.* **2014**, *71*, 153–163. [[CrossRef](#)]
14. Frechard, J.; Knittel, D. Drive requirements for elastic web roll-to-roll systems. *Mech. Mach. Theory* **2013**, *66*, 14–31. [[CrossRef](#)]
15. Martz, Y.; Ba, A.; Knittel, D. Robust industrial control with optimized decoupling in roll-to-roll systems: New approaches using finite element modeling of the Web. In Proceedings of the 2015 IEEE 20th Conference on Emerging Technologies & Factory Automation (ETFA), Luxembourg, 8–11 September 2015; pp. 1–4.
16. Torres, E.; Pagilla, P.R. Temperature Distribution in Moving Webs Heated by Radiation Panels: Model development and experimental validation. *J. Dyn. Syst. Meas. Control* **2017**, *139*, 051003. [[CrossRef](#)]
17. Torres, E.; Pagilla, P.R. A governing equation for moving web temperature heated by radiative panels. In Proceedings of the 2016 American Control Conference (ACC), Boston, MA, USA, 6–8 July 2016; pp. 858–863.
18. Lee, C.; Kang, H.; Shin, K. A study on tension behavior considering thermal effects in roll-to-roll E-printing. *J. Mech. Sci. Technol.* **2010**, *24*, 1097–1103. [[CrossRef](#)]
19. Lee, J.; Shin, K.; Lee, C. Analysis of dynamic thermal characteristic of register of roll-to-roll multi-layer printing systems. *Rob. Comput. Integr. Manuf.* **2015**, *35*, 77–83. [[CrossRef](#)]

